Scaling Tests of the Cross Section for Deeply Virtual Compton Scattering

C. Muñoz Camacho,[1] A. Camsonne,[2] M. Mazouz,[3] C. Ferdi,[2] G. Gavalian,[4] E. Kuchina,[5] M. Amarian,[4] K. A. Aniol,[6] M. Beaumel,[1] H. Benaoum,[7] P. Bertin,[2,8] M. Brossard,[2] J.-P. Chen,[8] E. Chudakov,[8] B. Craver,[9] F. Cusanno,[10] C. W. de Jager,[8] A. Deur,[8] R. Feuerbach,[8] J.-M. Fieschi,[2] S. Frullani,[10] M. Garçon,[1] F. Garibaldi,[10] O. Gayou,[11] R. Gilman,[5] J. Gomez,[8] P. Gueye,[12] P. A. M. Guichon,[1] B. Guillon,[3] O. Hansen,[8] D. Hayes,[4] D. Higinbotham,[8] T. Holmstrom,[13] C. E. Hyde-Wright,[4] H. Ibrahim,[4] R. Igarashi,[14] X. Jiang,[5] H. S. Jo,[15] L. J. Kaufman,[16] A. Kelleher,[13] A. Kolarkar,[17] G. Kumbartzki,[5] G. Laveissière,[2] J. J. LeRose,[8] R. Lindgren,[9] N. Liyanage,[9] H.-J. Lu,[18] D. J. Margaziotis,[6] Z.-E. Meziani,[19] K. McCormick,[5] R. Michaels,[8] B. Michel,[2] B. Moffit,[13] P. Monaghan,[11] S. Nanda,[8] V. Nelyubin,[9] M. Potokar,[20] Y. Qiang,[11] R. D. Ransome,[5] J.-S. Réal,[3] B. Reitz,[8] Y. Roblin,[8] J. Roche,[8] F. Sabatié,[1] A. Saha,[8] S. Sirca,[20] K. Slifer,[9] P. Solvignon,[19] R. Subedi,[21] V. Sulkosky,[13] P. E. Ulmer,[4] E. Voutier,[3] K. Wang,[9] L. B. Weinstein,[4] B. Wojtsekhowski,[8] X. Zheng,[22] and L. Zhu[23]

(Jefferson Lab Hall A Collaboration)

[1]*CEA Saclay, DAPNIA/SPhN, F-91191 Gif-sur-Yvette, France*
[2]*Université Blaise Pascal/CNRS-IN2P3, F-63177 Aubière, France*
[3]*Laboratoire de Physique Subatomique et de Cosmologie, 38026 Grenoble, France*
[4]*Old Dominion University, Norfolk, Virginia 23508, USA*
[5]*Rutgers, The State University of New Jersey, Piscataway, New Jersey 08854, USA*
[6]*California State University, Los Angeles, Los Angeles, California 90032, USA*
[7]*Syracuse University, Syracuse, New York 13244, USA*
[8]*Thomas Jefferson National Accelerator Facility, Newport News, Virginia 23606, USA*
[9]*University of Virginia, Charlottesville, Virginia 22904, USA*
[10]*INFN/Sezione Sanità, 00161 Roma, Italy*
[11]*Massachusetts Institute of Technology, Cambridge, Massachusetts 02139, USA*
[12]*Hampton University, Hampton, Virginia 23668, USA*
[13]*College of William and Mary, Williamsburg, Virginia 23187, USA*
[14]*University of Saskatchewan, Saskatchewan, Saskatchewan, Canada, S7N 5C6*
[15]*Institut de Physique Nucléaire CNRS-IN2P3, Orsay, France*
[16]*University of Massachusetts Amherst, Amherst, Massachusetts 01003, USA*
[17]*University of Kentucky, Lexington, Kentucky 40506, USA*
[18]*Department of Modern Physics, University of Science and Technology of China, Hefei 230026, China*
[19]*Temple University, Philadelphia, Pennsylvania 19122, USA*
[20]*Institut Jozef Stefan, University of Ljubljana, Ljubljana, Slovenia*
[21]*Kent State University, Kent, Ohio 44242, USA*
[22]*Argonne National Laboratory, Argonne, Illinois, 60439, USA*
[23]*University of Illinois, Urbana, Illinois 61801, USA*

(Received 26 July 2006; published 29 December 2006)

We present the first measurements of the $\vec{e}p \to ep\gamma$ cross section in the deeply virtual Compton scattering (DVCS) regime and the valence quark region. The Q^2 dependence (from 1.5 to 2.3 GeV^2) of the helicity-dependent cross section indicates the twist-2 dominance of DVCS, proving that generalized parton distributions (GPDs) are accessible to experiment at moderate Q^2. The helicity-independent cross section is also measured at $Q^2 = 2.3$ GeV^2. We present the first model-independent measurement of linear combinations of GPDs and GPD integrals up to the twist-3 approximation.

DOI: 10.1103/PhysRevLett.97.262002 PACS numbers: 13.60.Fz, 13.40.Gp, 13.60.Hb, 14.20.Dh

Measurements of electroweak form factors determine nucleon spatial structure, and deep inelastic scattering (DIS) of leptons off the nucleon measures parton distribution functions, which determine longitudinal momentum distributions. The demonstration by Ji [1], Radyushkin [2], and Mueller *et al.* [3], of a formalism to relate the spatial and momentum distributions of the partons allows the exciting possibility of determining spatial distributions of quarks and gluons in the nucleon as a function of the parton wavelength. These new structure functions, now called generalized parton distributions (GPD), became of experimental interest when it was shown [1] that they are accessible through deeply virtual Compton scattering (DVCS) and its interference with the Bethe-Heitler (BH) process (Fig. 1). Figure 1 presents our kinematic nomenclature. DVCS is defined kinematically by the

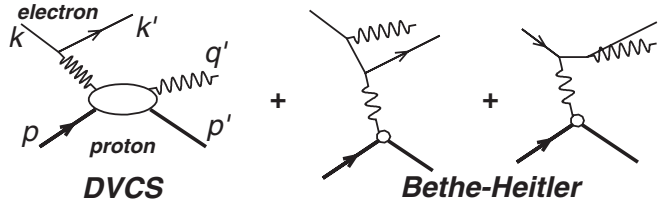

FIG. 1. Lowest-order QED diagrams for the process $ep \to ep\gamma$, including the DVCS and Bethe-Heitler (BH) amplitudes. The external momentum four-vectors are defined on the diagram. The virtual photon momenta are $q = k - k'$ in the DVCS- and $\Delta = q - q'$ in the BH-amplitudes. The invariants are: $W^2 = (q + p)^2$, $Q^2 = -q^2 > 0$, $t = \Delta^2$, $x_{\rm Bj} = Q^2/(2p \cdot q)$, and the DVCS scaling variable $\xi = -\bar{q}^2/(\bar{q} \cdot P) \approx x_{\rm Bj}/(2 - x_{\rm Bj})$, with $\bar{q} = (q + q')/2$ and $P = p + p'$.

limit $-t \ll Q^2$ and Q^2 much larger than the quark confinement scale.

The factorization proofs [4,5] confirmed the connection between DVCS and DIS. Diehl *et al.* [6] showed that the twist-2 and twist-3 contributions in the DVCS-BH interference terms (the first two leading orders in $1/Q$) could be extracted independently from the azimuthal dependence of the helicity-dependent cross section. Burkardt [7] showed that the t dependence of the GPDs is the Fourier conjugate to the transverse spatial distribution of quarks in the infinite momentum frame as a function of momentum fraction. Ralston and Pire [8], Diehl [9], and Belitsky *et al.* [10] extended this interpretation to the general case of skewness $\xi \neq 0$. The light-cone wave function representation by Brodsky *et al.* [11] allows GPDs to be interpreted as interference terms of wave functions for different parton configurations in a hadron.

These concepts stimulated an intense experimental effort in DVCS. The H1 [12,13] and ZEUS [14] Collaborations measured the cross section for $x_{\rm Bj} \approx 10^{-3}$. The HERMES Collaboration measured relative beam helicity [15] and beam-charge asymmetries [16,17]. Relative beam helicity [18] and longitudinal target [19] asymmetries were measured at the Thomas Jefferson National Accelerator Facility (JLab) by the CLAS Collaboration.

Extracting GPDs from DVCS requires the fundamental demonstration that DVCS is well described by the twist-2 diagram of Fig. 1 at finite Q^2. This Letter reports the first strong evidence of this cornerstone hypothesis, necessary to validate all previous and future GPD measurements using DVCS. We present the determination of the cross section of the $\vec{e}p \to ep\gamma$ reaction for positive and negative electron helicity in the kinematics of Table I.

The E00-110 [20] experiment ran in Hall A [21] at JLab. The 5.75 GeV electron beam was incident on a 15 cm liquid H_2 target. Our typical luminosity was $10^{37}/{\rm cm}^2/{\rm s}$ with 76% beam polarization. We detected scattered electrons in one high resolution spectrometer (HRS). Photons above a 1 GeV energy threshold (and $\gamma\gamma$ coincidences from π^0 decay) were detected in a 11×12 array of $3 \times 3 \times 18.6$ cm^3 PbF_2 crystals, whose front face was located 110 cm from the target center. We calibrated the PbF_2 array by coincident elastic $H(e, e'_{\rm Calo} p_{\rm HRS})$ data. With (elastic) $k' = 4.2$ GeV/c, we obtain a PbF_2 resolution of 2.4% in energy and 2 mm in transverse position (one-σ). The calibration was monitored by reconstruction of the $\pi^0 \to \gamma\gamma$ mass from $H(e, e'\pi^0)X$ events.

We present in Fig. 2 the missing mass squared obtained for $H(e, e'\gamma)X$ events, with coincident electron-photon detection. After subtraction of an accidental coincidence sample, we have the following competing channels in addition to $H(e, e'\gamma)p$: $ep \to e\pi^0 p$, $ep \to e\pi^0 N\pi$, $ep \to e\gamma N\pi$, $ep \to e\gamma N\pi\pi \ldots$. From symmetric (lab-frame) π^0 decay, we obtain a high statistics sample of $H(e, e'\pi^0)X'$ events, with two photon clusters in the PbF_2 calorimeter. From these events, we determine the statistical sample of (asymmetric) $H(e, e'\gamma)\gamma X'$ events that must be present in our $H(e, e'\gamma)X$ data. The solid M_X^2 spectrum displayed in Fig. 2 was obtained after subtracting this π^0 yield from the total (stars) distribution. This is a 14% average subtraction in the exclusive window defined by M_X^2 cut in Fig. 2. Depending on the bin in $\phi_{\gamma\gamma}$ and t, this subtraction varies from 6% to 29%. After our π^0 subtraction, the only remaining channels, of type $H(e, e'\gamma)N\pi$, $N\pi\pi$, etc. are kinematically constrained to $M_X^2 > (M + m_\pi)^2$. This is the value (M_X^2 cut in Fig. 2) we chose for truncating our integration. Resolution effects can cause the inclusive channels to contribute below this cut. To evaluate this possible contamination, we used an additional proton array (PA) of 100 plastic scintillators. The PA subtended a solid angle (relative to the nominal direction of the $\mathbf{q}$ vector) of $18° < \theta_{\gamma p} < 38°$ and $45° < \phi_{\gamma p} = 180° - \phi_{\gamma\gamma} < 315°$, arranged in 5 rings of 20 detectors. For $H(e, e'\gamma)X$ events near the exclusive region, we can predict which block in the PA should have a signal from a proton from an exclusive $H(e, e'\gamma p)$ event. Open crosses

TABLE I. Experimental $ep \to ep\gamma$ kinematics, for incident beam energy $E = 5.75$ GeV. θ_q is the central value of the $\mathbf{q}$-vector direction. The PbF_2 calorimeter was centered on θ_q for each setting. The photon energy for $\mathbf{q}' \parallel \mathbf{q}$ is E_γ.

Kin	k' (GeV/c)	θ_e (°)	Q^2 (GeV^2)	$x_{\rm Bj}$	θ_q (°)	W (GeV)	E_γ (GeV)
1	3.53	15.6	1.5	0.36	−22.3	1.9	2.14
2	2.94	19.3	1.9	0.36	−18.3	2.0	2.73
3	2.34	23.8	2.3	0.36	−14.8	2.2	3.33

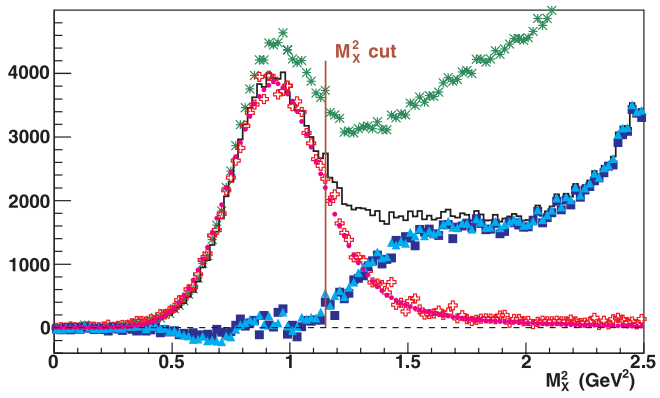

FIG. 2 (color online). Missing mass squared for $H(e, e'\gamma)X$ events (stars) at $Q^2 = 2.3$ GeV^2 and $-t \in [0.12, 0.4]$ GeV^2, integrated over the azimuthal angle of the photon $\phi_{\gamma\gamma}$. The solid histogram shows the data once the $H(e, e'\gamma)\gamma X'$ events have been subtracted. The other histograms are described in the text.

show the $X = (p + y)$ missing mass squared distribution for $H(e, e'\gamma p)y$ events in the predicted PA block, with a signal above an effective threshold 30 MeV. Squares show our inclusive yield, obtained by subtracting the normalized triple coincidence yield from the $H(e, e'\gamma)X$ yield. The dotted curve shows our simulated $H(e, e'\gamma)p$ spectrum, including radiative and resolution effects, normalized to fit the data for $M_X^2 \leq M^2$. Triangles show the estimated inclusive yield obtained by subtracting the simulation from the data. Squares and triangles are in good agreement, and show that our exclusive yield has less than 3% contamination from inclusive processes.

To order twist-3 the DVCS helicity-dependent ($d\Sigma$) and helicity-independent ($d\sigma$) cross sections are [22]:

$$\frac{d^4\Sigma}{d^4\Phi} = \frac{1}{2}\left[\frac{d^4\sigma^+}{d^4\Phi} - \frac{d^4\sigma^-}{d^4\Phi}\right] = \frac{d^4\Sigma(|\mathrm{DVCS}|^2)}{d^4\Phi} + \sin(\phi_{\gamma\gamma})\Gamma_1^{\mathrm{Im}}\mathrm{Im}[\mathcal{C}^I(\mathcal{F})] - \sin(2\phi_{\gamma\gamma})\Gamma_2^{\mathrm{Im}}\mathrm{Im}[\mathcal{C}^I(\mathcal{F}^{\mathrm{eff}})], \quad (1)$$

$$\frac{d^4\sigma}{d^4\Phi} = \frac{1}{2}\left[\frac{d^4\sigma^+}{d^4\Phi} + \frac{d^4\sigma^-}{d^4\Phi}\right] = \frac{d^4\sigma(|\mathrm{DVCS}|^2)}{d^4\Phi} + \frac{d^4\sigma(|\mathrm{BH}|^2)}{d^4\Phi} + \Gamma_{0,\Delta}^{\mathrm{Re}}\mathrm{Re}[\mathcal{C}^I + \Delta\mathcal{C}^I](\mathcal{F}) + \Gamma_0^{\mathrm{Re}}\mathrm{Re}[\mathcal{C}^I(\mathcal{F})] - \cos(\phi_{\gamma\gamma})\Gamma_1^{\mathrm{Re}}\mathrm{Re}[\mathcal{C}^I(\mathcal{F})] + \cos(2\phi_{\gamma\gamma})\Gamma_2^{\mathrm{Re}}\mathrm{Re}[\mathcal{C}^I(\mathcal{F}^{\mathrm{eff}})], \quad (2)$$

where $d^4\Phi = dQ^2 dx_{\mathrm{Bj}} dt d\phi_{\gamma\gamma}$ and the azimutal angle $\phi_{\gamma\gamma}$ of the detected photon follows the "Trento Convention" [23]. The $\Gamma_n^{\mathrm{Re,Im}}$ are kinematic factors with a $\phi_{\gamma\gamma}$ dependence that arises from the electron propagators of the BH amplitude. The $\mathcal{C}^I$ and $\Delta\mathcal{C}^I$ angular harmonics depend on the interference of the BH amplitude with the set $\mathcal{F} = \{\mathcal{H}, \mathcal{E}, \tilde{\mathcal{H}}, \tilde{\mathcal{E}}\}$ of twist-2 Compton form factors (CFFs) or the related set $\mathcal{F}^{\mathrm{eff}}$ of effective twist-3 CFFs:

$$\mathcal{C}^I(\mathcal{F}) = F_1\mathcal{H} + \xi G_M\tilde{\mathcal{H}} - \frac{t}{4M^2}F_2\mathcal{E}, \quad (3)$$

$$\mathcal{C}^I(\mathcal{F}^{\mathrm{eff}}) = F_1\mathcal{H}^{\mathrm{eff}} + \xi G_M\tilde{\mathcal{H}}^{\mathrm{eff}} - \frac{t}{4M^2}F_2\mathcal{E}^{\mathrm{eff}}, \quad (4)$$

$$[\mathcal{C}^I + \Delta\mathcal{C}^I](\mathcal{F}) = F_1\mathcal{H} - \frac{t}{4M^2}F_2\mathcal{E} - \xi^2 G_M[\mathcal{H} + \mathcal{E}]. \quad (5)$$

$F_1(t)$, $F_2(t)$, and $G_M(t) = F_1(t) + F_2(t)$ are the elastic form factors. CFFs are defined in terms of the GPDs H_f, E_f, $\tilde{H}_f$, and $\tilde{E}_f$, defined for each quark flavor f. For example, ($f \in \{u, d, s\}$):

$$\mathcal{H}(\xi, t) = \sum_f \left[\frac{e_f}{e}\right]^2 \left\{ i\pi[H_f(\xi, \xi, t) - H_f(-\xi, \xi, t)] + \mathcal{P}\int_{-1}^{+1} dx\left[\frac{2x}{\xi^2 - x^2}\right]H_f(x, \xi, t)\right\}. \quad (6)$$

Thus, the DVCS helicity-dependent and helicity-independent cross sections provide very distinct and complementary information on GPDs. On one hand, $d\Sigma$ measures the imaginary part of the BH-DVCS interference terms and provides direct access to GPDs at $x = \xi$. On the other hand, $d\sigma$ determines the real part of the BH-DVCS interference terms and measures the integral of GPDs over their full domain in x. This real part of the BH-DVCS interference term is the same interference term that can be obtained by measurements of the difference of electron and positron (or $\mu^{\pm}$) DVCS cross sections.

The twist-2 and twist-3 CFFs are matrix elements of quark-gluon operators and are independent of Q^2 (up to logarithmic QCD evolution). Their Q^2 variation measures the potential contamination from higher twists.

The helicity-independent cross section also has a $\cos(3\phi_{\gamma\gamma})$ twist-2 gluon transversity term. We expect this term to be small, and do not include it in our analysis. We neglect the DVCS^2 terms in our analysis. Therefore, our results for $\mathrm{Im}[\mathcal{C}^I]$ and $\mathrm{Re}[\mathcal{C}^I]$ may contain, respectively, twist-3 and twist-2 DVCS^2 terms, which enter with similar $\phi_{\gamma\gamma}$ dependence. However, the DVCS^2 terms in both $d\sigma$ and $d\Sigma$ are kinematically suppressed by at least an order of magnitude in our kinematics [22], because they are not enhanced by the BH amplitude. In any case, the terms we neglect do not affect the cross sections we extract, which are accurately parametrized, within statistics, by the contributions we included.

Our simulation includes internal bremsstrahlung in the scattering process and external bremsstrahlung and ionization straggling in the target and scattering chamber win-

TABLE II. Angular harmonics fit results, Im and Re parts, and their statistical uncertainties.

$Q^2\backslash\langle t\rangle$ (GeV^2)		$t = -0.33$	-0.28	-0.23	-0.17
Im	1.5	2.1 ± 0.3	2.1 ± 0.3	2.0 ± 0.2	3.2 ± 0.2
$[\mathcal{C}^I(\mathcal{F})]$	1.9	1.9 ± 0.2	2.3 ± 0.2	2.5 ± 0.2	3.2 ± 0.2
	2.3	2.1 ± 0.2	2.4 ± 0.2	2.6 ± 0.2	3.3 ± 0.3
Im	1.5	2.8 ± 2.0	2.5 ± 2.0	0.1 ± 2.1	0.6 ± 2.4
$[\mathcal{C}^I(\mathcal{F}^{\rm eff})]$	1.9	0.3 ± 1.4	3.8 ± 1.5	-0.9 ± 1.8	4.7 ± 2.7
	2.3	5.3 ± 1.6	0.7 ± 1.8	0.2 ± 2.5	4.0 ± 4.6
		$Q^2 = 2.3$ GeV^2, Re part of angular harmonics			
$\mathcal{C}(\mathcal{F})$		-2.4 ± 0.1	-2.0 ± 0.1	-1.7 ± 0.1	-0.7 ± 0.2
$[\mathcal{C} + \Delta\mathcal{C}](\mathcal{F})$		0.1 ± 0.1	0.8 ± 0.1	1.6 ± 0.1	2.5 ± 0.1
$[\mathcal{C}(\mathcal{F}^{\rm eff})]$		-1.4 ± 0.5	0.6 ± 0.6	1.0 ± 0.8	3.4 ± 1.4

dows. We include spectrometer resolution and acceptance effects and a full GEANT3 simulation of the detector response to the DVCS photons and protons. The spectrometer acceptance is defined for both the data and simulation by a R-function cut [24]. Radiative corrections for virtual photons and unresolved real photons are applied according to the VCS (BH + Born amplitude) specific prescriptions of Ref. [25]. This results in a global correction factor (independent of $\phi_{\gamma\gamma}$ or helicity) of 0.91 ± 0.02 applied to our experimental yields. Within the quoted uncertainty, this correction is independent of the kinematic setting.

For each (Q^2, $x_{\rm Bj}$, t) bin, we fit the Re and Im parts (as appropriate) of the harmonics $\mathcal{C}_n \in \{\mathcal{C}^I(\mathcal{F}), \mathcal{C}^I(\mathcal{F}^{\rm eff}), [\mathcal{C}^I + \Delta\mathcal{C}^I](\mathcal{F})\}$ as independent parameters. In Kin-1 and Kin-2, due to the lower photon energy E_γ (Table I), our acceptance, trigger, and readout did not record a comprehensive set of $ep \to e\pi^0 X$ events. For those events we were able to reconstruct, we found only a few percent contribution to $d\Sigma$, but a larger contribution to $d\sigma$. For Kin-1,2, we only present results on $d\Sigma$. Our systematic errors in the cross-section measurements are dominated by the following contributions: 3% from HRS $\times$ PbF_2 acceptance and luminosity; 3% from $H(e, e'\gamma)\gamma X$ (π^0) background; 2% from radiative corrections; and 3% from inclusive $H(e, e'\gamma)N\pi\ldots$ background. The total, added in quadrature, is 5.6%. The $d\Sigma$ results contain an additional 2% systematic uncertainty from the beam polarization. In order to compute the BH contribution in the $d\sigma$ analysis we used Kelly's parametrization of form factors [26], which reproduce elastic cross-section world data in our t range with 1% error and 90% C.L.

For one (Q^2, $x_{\rm Bj}$, t) bin, Fig. 3 shows the helicity-dependent and helicity-independent cross sections, respectively. We notice that the twist-3 terms make only a very small contribution to the cross sections. Note also that $d\sigma$ is much larger than the BH contribution alone, especially from 90° to 270°. This indicates that the relative beam spin asymmetry BSA $= d^4\Sigma/d^4\sigma$ cannot be simply equated to the imaginary part of the BH-DVCS interference divided by the BH cross section. Table II lists the extracted angular harmonics. Figure 4 (left) shows the Q^2 dependence of the imaginary angular harmonic $\mathrm{Im}[\mathcal{C}^I]$ over our full t domain, with $\langle t\rangle = -0.25$ GeV^2 ($\langle t\rangle$ varying by ± 0.01 GeV^2 over Kin 1-3).

The absence of Q^2 dependence of $\mathrm{Im}[\mathcal{C}^I(\mathcal{F})]$ within its 3% statistical uncertainty provides crucial support for the dominance of twist-2 in the DVCS amplitude. Indeed, it sets an upper limit $\leq 10\%$ to twist-4 and higher contributions. $\mathrm{Im}[\mathcal{C}^I(\mathcal{F})]$ is thereby a direct measurement of a linear combination of GPDs. The two twist-2 angular harmonics extracted from $d\sigma$ determine distinct combinations of GPD integrals, providing most valuable complementary information on GPDs. As noted above, the angular

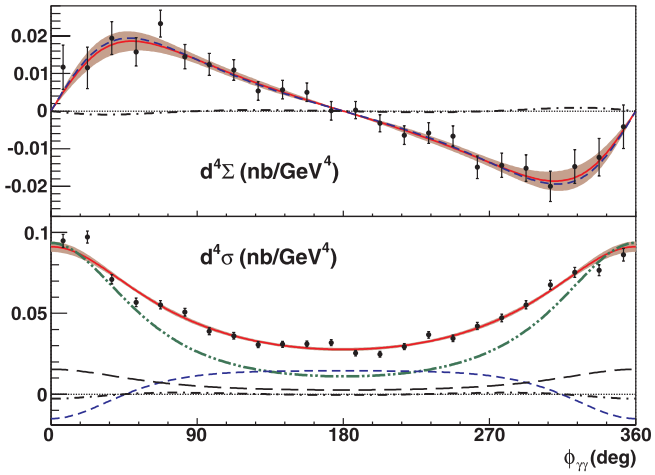

FIG. 3 (color online). Data and fit to $d^4\Sigma/[dQ^2 dx_{\rm Bj} dt d\phi_{\gamma\gamma}]$, and $d^4\sigma/[dQ^2 dx_{\rm Bj} dt d\phi_{\gamma\gamma}]$, as a function of $\phi_{\gamma\gamma}$. Both are in the bin $\langle Q^2, t\rangle = (2.3, -0.28)$ GeV^2 at $\langle x_{\rm Bj}\rangle = 0.36$. Error bars show statistical uncertainties. Solid lines show total fits with one-σ statistical error bands. Systematic uncertainty is given in the text. The dot-dot-dashed line is the $|\mathrm{BH}|^2$ contribution to $d^4\sigma$. The short-dashed lines in $d^4\Sigma$ and $d^4\sigma$ are the fitted Im and Re parts of $\mathcal{C}^I(\mathcal{F})$, respectively. The long-dashed line is the fitted $\mathrm{Re}[\mathcal{C}^I + \Delta\mathcal{C}^I](\mathcal{F})$ term. The dot-dashed curves are the fitted Im and Re parts of $\mathcal{C}^I(\mathcal{F}^{\rm eff})$.

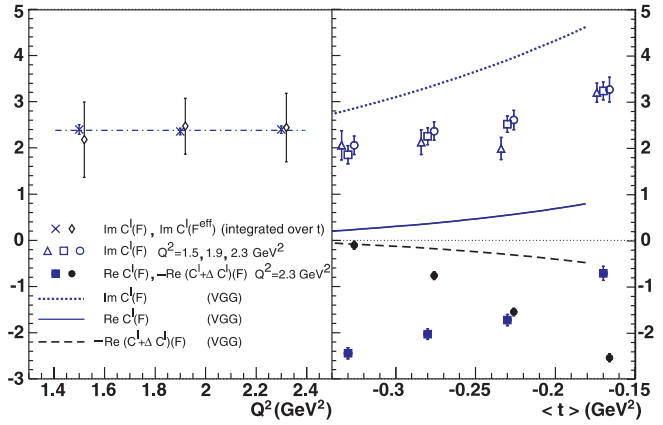

FIG. 4 (color online). Left: Q^2 dependence of Im parts of (twist-2) $\mathcal{C}^I(\mathcal{F})$ and (twist-3) $\mathcal{C}^I(\mathcal{F}^{\text{eff}})$ angular harmonics, averaged over t. The horizontal line is the fitted average of $\text{Im}[\mathcal{C}^I(\mathcal{F})]$. Right: Extracted real and imaginary parts of the twist-2 angular harmonics as functions of t. The VGG model curves are described in the text. Note the sign of $-[\mathcal{C}^I + \Delta\mathcal{C}^I] \times (\mathcal{F})$ (data and VGG). Superposed points in both panels are offset for visual clarity. Their error bars show statistical uncertainties.

harmonic terms in Table II may include contributions from kinematically suppressed bilinear DVCS^2 terms omitted in our analysis. In our experiment the acceptance-averaged ratios of the kinematic coefficients of the DVCS^2 terms to the BH-DVCS terms are below 1.2% for $d\Sigma$ and below 4.5% for $d\sigma$. The cross-section measurements we present are accurate, to the quoted uncertainty, and not sensitive within statistics to the neglected terms in their harmonic analysis.

Figure 4 (right) displays the twist-2 angular harmonics of Table II (Re and Im parts) as functions of t, together with the predictions from a model by Vanderhaeghen, Guichon, and Guidal (VGG) [27–29]. The VGG model (twist-2 contribution only, profile parameter $b_{\text{val}} = b_{\text{sea}} = 1$, Regge parameter $\alpha' = 0.8\ \text{GeV}^{-2}$, GPD $E_f = 0$) is in qualitative agreement with the $\text{Im}[\mathcal{C}^I(\mathcal{F})]$ data, but significantly underpredicts the principal-value integrals (Re parts of the angular harmonics).

In summary, we present the first explicit demonstration of exclusivity in DVCS kinematics. We also present the first measurements of DVCS cross section in the valence quark region. From the Q^2 dependence of the angular harmonics of the helicity-dependent cross section, we provide solid evidence of twist-2 dominance in DVCS, which makes GPDs accessible to experiment even at modest Q^2. This result supports the striking prediction of perturbative QCD scaling in DVCS [1,2]. As a consequence of this evidence for scaling in the exclusive channel, and our separate determination of the helicity-dependent and helicity-independent cross sections, we extract for the first time a model-independent combination of GPDs and GPDs integrals.

We acknowledge essential work of the JLab accelerator staff and the Hall A technical staff. This work was supported by DOE Contract No. DOE-AC05-06OR23177 under which the Jefferson Science Associates, LLC, operates the Thomas Jefferson National Accelerator Facility. We acknowledge additional grants from the DOE and NSF and the CNRS and Commissariat à l'Energie Atomique.

[1] X. Ji, Phys. Rev. Lett. **78**, 610 (1997).
[2] A. V. Radyushkin, Phys. Rev. D **56**, 5524 (1997).
[3] D. Mueller, D. Robaschik, B. Geyer, F. M. Dittes, and J. Horejsi, Fortschr. Phys. **42**, 101 (1994).
[4] J. C. Collins and A. Freund, Phys. Rev. D **59**, 074009 (1999).
[5] X. Ji and J. Osborne, Phys. Rev. D **58**, 094018 (1998).
[6] M. Diehl, T. Gousset, B. Pire, and J. P. Ralston, Phys. Lett. B **411**, 193 (1997).
[7] M. Burkardt, Phys. Rev. D **62**, 071503(R) (2000).
[8] J. P. Ralston and B. Pire, Phys. Rev. D **66**, 111501(R) (2002).
[9] M. Diehl, Eur. Phys. J. C **25**, 223 (2002).
[10] A. V. Belitsky, X. Ji, and F. Yuan, Phys. Rev. D **69**, 074014 (2004).
[11] S. J. Brodsky, M. Diehl, and D. S. Hwang, Nucl. Phys. **B596**, 99 (2001).
[12] A. Aktas *et al.* (H1 Collaboration), Eur. Phys. J. C **44**, 1 (2005).
[13] C. Adloff *et al.* (H1 Collaboration), Phys. Lett. B **517**, 47 (2001).
[14] S. Chekanov *et al.* (ZEUS Collaboration), Phys. Lett. B **573**, 46 (2003).
[15] A. Airapetian *et al.* (HERMES Collaboration), Phys. Rev. Lett. **87**, 182001 (2001).
[16] F. Ellinghaus (HERMES Collaboration), Nucl. Phys. **A711**, 171 (2002).
[17] A. Airapetian *et al.* (HERMES Collaboration), hep-ex/0605108.
[18] S. Stepanyan *et al.* (CLAS Collaboration), Phys. Rev. Lett. **87**, 182002 (2001).
[19] S. Chen *et al.* (CLAS Collaboration), Phys. Rev. Lett. **97**, 072002 (2006).
[20] URL http://hallaweb.jlab.org/experiment/DVCS
[21] J. Alcorn *et al.*, Nucl. Instrum. Methods Phys. Res., Sect. A **522**, 294 (2004).
[22] A. V. Belitsky, D. Mueller, and A. Kirchner, Nucl. Phys. **B629**, 323 (2002).
[23] A. Bacchetta, U. D'Alesio, M. Diehl, and C. A. Miller, Phys. Rev. D **70**, 117504 (2004).
[24] M. Rvachev, Hall A Technical Note JLab-TN-01-055, Jefferson Lab (2001).
[25] M. Vanderhaeghen *et al.*, Phys. Rev. C **62**, 025501 (2000).
[26] J. J. Kelly, Phys. Rev. C **70**, 068202 (2004).
[27] M. Vanderhaeghen, P. A. M. Guichon, and M. Guidal, Phys. Rev. D **60**, 094017 (1999).
[28] K. Goeke, M. V. Polyakov, and M. Vanderhaeghen, Prog. Part. Nucl. Phys. **47**, 401 (2001).
[29] M. Guidal, M. V. Polyakov, A. V. Radyushkin, and M. Vanderhaeghen, Phys. Rev. D **72**, 054013 (2005).